Colloidal Synthesis of Cu-M-S (M=V, Cr, Mn) Nanocrystals by Tuning the Copper Precursor Reactivity

Valeria Mantella[a], Seyedeh Behnaz Varandili[a], James R. Pankhurst[a], Raffaella Buonsanti[a*]

Laboratory of Nanochemistry for Energy (LNCE), Department of Chemical Sciences and Engineering, École Polytechnique Fédérale de Lausanne, CH-1950 Sion, Switzerland.

* Corresponding author: raffaella.buonsanti@epfl.ch

ABSTRACT

New ternary and higher order inorganic materials are needed for a large variety of applications, yet their synthesis still represent a chemistry challenge. Herein, we focus on the synthesis of Cu-M-S nanocrystals (where M = V, Cr, Mn) via a wet-chemistry route and investigate their formation mechanisms. We reveal that the interplay between the copper precursor and the thiophilicity of the transition metal M is key for the synthesis of pure phase Cu-M-S nanocrystals under the same reaction conditions. In particular, we observe that the interdiffusion kinetics of the intermediate species are crucial and the extent of nucleation of the ternary product can be controlled by the copper precursor reactivity. The insights provided by this work open up new avenues toward the design of improved synthesis strategies to multinary nanocrystalline compounds.

INTRODUCTION

Materials chemists have delved into the synthesis of copper-based multinary nanomaterials in response to an increasing demand for novel properties serving applications which span from energy to biotechnology.[1–9] One notable example of such intense research is represented by copper-based chalcogenide nanocrystals (NCs), such as the Cu-III-VI, Cu-IV-VI, and Cu-V-VI families, whereby a superior control over their structure and composition has been achieved by means of colloidal chemistry.[1–9] As a result, their physicochemical and functional properties have been investigated and exploited for more than two decades.[1–9] However, the synthetic library of copper-based multinary NCs is far from being complete. Indeed, if all the

possible chemical substitutions and structural modifications attainable in complex compositions are taken into account, one soon realizes that there is still plenty of room for the discovery of new materials. For instance, Cu-M-S/Se NCs where M is a transition metal, have been show to possess very interesting optical properties because of their peculiar band structure.[10,11] However, only few of these have been synthesized so far. [12–16]

One of the major bottlenecks to obtain novel multinary systems is the complexity of the synthesis itself. Indeed, as the number of elements increases, different chemical interactions might arise during the formation of the targeted compounds. Therefore, choosing the reaction conditions and identifying the parameters which ensure the formation of the pure-phase materials is not trivial. In kinetically-driven approaches, like colloidal chemistry, slight variations in the chemical potential of the species involved in the nucleation and growth stages might result in the formation of undesired reaction byproducts, such as binary compounds.[4,17] Overall, guidelines for the synthesis of multinary NCs are still missing.

Herein, we report a solution-phase synthesis of Cu-M-S NCs, where M = V, Cr, Mn, under the same reaction conditions (i.e. temperature, reaction time, concentrations, solvent, surface ligands). X-Ray diffraction, transmission electron microscopy and compositional analysis confirm the phase purity of the obtained NCs. By careful analysis of the reaction intermediates, we discover that balancing the copper precursor reactivity with the thiophilicity of the M cation is a crucial parameter to control the reaction pathway and obtain phase pure NCs with decent size monodispersity.

EXPERIMENTAL SECTION

General

All glassware was oven dried prior to use. Standard Schlenk line techniques assisted by a nitrogen-filled glovebox were used for all the synthesis. A J-KEM Scientific model 310 temperature controller was used with a heating mantle for reaction temperature control.

Chemicals

Copper(I) iodide (CuI, 98%), copper (I) acetate (Cu(OAc), 97%), copper (II) acetylacetonate ($Cu(acac)_2$, 97%), vanadium acetylacetonate ($V(acac)_3$ 97%) chromium

acetylacetonate ($Cr(acac)_3$, 97%), manganese acetylacetonate ($Mn(acac)_3$, 97%) oleylamine (OLAM, technical grade, 70%), 1-octadecene (ODE, technical grade, 90%), 1-dodecanethiol (DDT, technical grade 98%), and ethanol (anhydrous) were all purchased from Sigma-Aldrich and used as received without further purification. Hexane (anhydrous, 95%) was purchased from TCI Deutschland GmbH.

Synthesis of Cu_3VS_4 nanocrystals

Cu_3VS_4 NCs were obtained by slightly modifying the synthetic protocol previously reported by us.[12] Specifically the trioctylphosphine was removed as no difference was observed in the reaction product with/o it. In a typical synthesis, Cu_3VS_4 NCs were obtained by introducing CuI (0.25 mmol, 0.05g) and $V(acac)_3$ (0.33mmol, 0.12g), dissolved in ODE (7 mL), in a 25 mL three-necked round-bottom flask under a protective atmosphere of nitrogen, which was maintained during the whole synthesis. The resulting mixture was stirred and heated up at 14 °C/min to 280°C. In the meanwhile, a vial containing both DDT (10 mmol, 2.395 mL) and OLAM (3 mmol, 1 mL) was kept under nitrogen at room temperature for 10 minutes. The resulting solution was swiftly injected into the metal precursor solution at the target temperature. After injection, the temperature was allowed to recover and the final solution was held at the target temperature for 30minutes. After that, the dark colloidal solution was allowed to cool down to room temperature by removing the heating mantle. The contents of the flask were divided into 2 × 50 mL centrifuge tubes; 20 mL of an ethanol/hexane mixture (1:1 v/v) was added to each of them. The product was collected by centrifugation at 5000 rpm for 15 minutes and resuspended in anhydrous hexane. After another precipitation/resuspension cycle with the same solvents, the NCs were suspended in anhydrous hexane and stored in the glovebox to preserve the colloidal stability.

Synthesis of $CuCrS_2$ nanocrystals

$CuCrS_2$ NCs were obtained by following the synthetic protocol reported for Cu_3VS_4 NCs. However, in a typical synthesis, $Cr(acac)_3$ (0.33mmol, 0.12g) was employed and CuI was substituted by Cu(OAc) (0.25mmol, 0.03g), while keeping the rest of the synthetic conditions and washing procedure.

Synthesis of Cu_2MnS_2 nanocrystals

Cu_2MnS_2 NCs were obtained by following the synthetic procedure reported for Cu_3VS_4 NCs. However, in a typical synthesis, $Mn(acac)_3$ (0.33mmol, 0.12g) was employed and

CuI was replaced by $Cu(acac)_2$ (0.25mmol, 0.065g), the rest of the reaction conditions as well as the washing procedure were kept the same.

Electron Microscopy

Transmission Electron Microscopy (TEM) images were recorded on an Analytical JEOL-2100F FETEM using a beam energy of 120 kV, equipped with a Gatan camera. Samples were drop-casted on a copper TEM grid (Ted Pella, Inc.) prior to imaging. Size statistics were performed using the software ImageJ and counting 200 particles per sample. Elemental mapping was performed on 10 particles per samples and the error on the atomic % estimated to be 0.1 %. High-resolution TEM (HR-TEM) images, STEM- HAADF (scanning transmission electron microscopy – high angle annular dark-field) images and corresponding EDXS (energy-dispersive X-ray spectroscopy) maps were acquired on a FEI Tecnai-Osiris using an accelerating of 200 kV. This microscope is equipped with a high brightness X-FEG gun, silicon drift Super-X-EDX detectors and a Bruker Esprit acquisition software.

X-Ray Diffraction (XRD) Analysis

The XRD patterns reported were acquired on a Bruker D8 Advance diffractometer with a Cu Kα source equipped with a Lynxeye one-dimensional detector. The diffractometer operated at 40 kV and 40 mA with a Cu Kα source with wavelength of $\lambda = 1.54$ Å. The samples were drop-casted on a silicon wafer, previously washed using acetone and isopropanol.

RESULTS AND DISCUSSION

Structural and Compositional Characterization of phase-pure ternary Cu-M-S NCs

We prepared phase-pure Cu_3VS_4, $CuCrS_2$ and Cu_2MnS_2 NCs using a colloidal hot-injection method. In a typical synthesis, a solution of DDT/ OLAM was swiftly injected at 280°C into a mixture containing CuI, Cu(OAc), or $Cu(acac)_2$, along with $V(acac)_3$, $Cr(acac)_3$, $Mn(acac)_3$), respectively, dissolved in ODE. TEM micrographs of the resulting samples show the formation of cubic, hexagonal or polyhedral shaped Cu_3VS_4 (19.1 ± 2.5 nm) $CuCrS_2$ (18.0 ± 2.0 nm) and Cu_2MnS_2 (20.2 ± 6.3 nm) NCs, (**Figure 1A-C, S1**). The crystalline phases were ascertained by means of XRD

analysis (**Figure 1D-F**), which reveals the pure cubic Cu_3VS_4 ($P\bar{4}3m$, a = 5.393(1) Å), hexagonal $CuCrS_2$ (R3(146), a=b= 3.483Å, c= 18.7Å) and cubic Cu_2MnS_2 (Fd-3m(227), a= 8.96Å) phases.

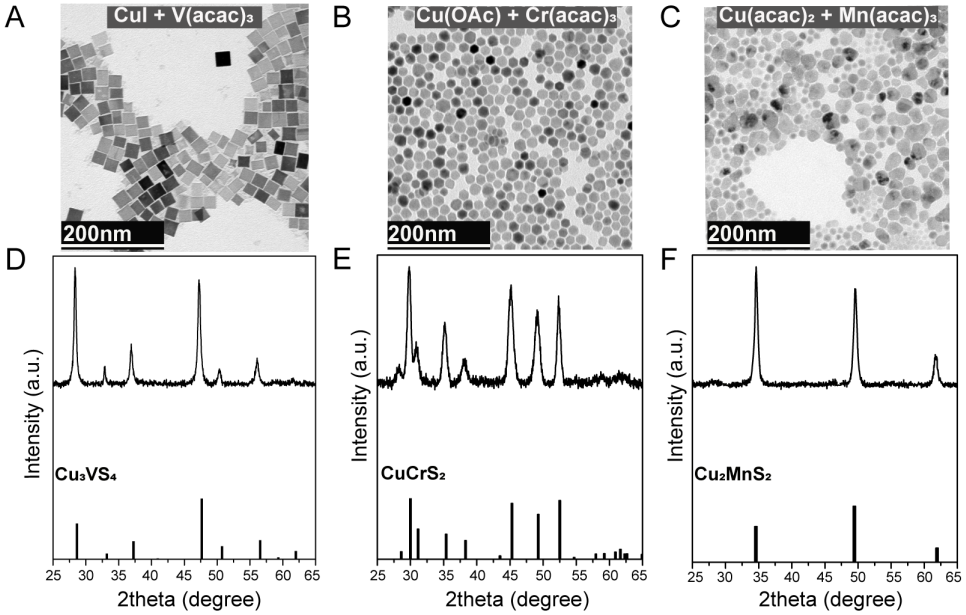

Figure 1. (A-C) Representative TEM images and (D-F) corresponding XRD patterns of pure Cu_3VS_4, $CuCrS_2$ and Cu_2MnS_2 colloidal NCs obtained after reacting CuI, Cu(OAc), $Cu(acac)_2$ (0.25mmol) along with $V(acac)_3$, $Cr(acac)_3$, $Mn(acac)_3$ (0.33mmol), respectively, at 280°C for 30minutes, in the presence of DDT (10mmol), OLAM (3mmol) in ODE (7 ml). The XRD reference patterns of Cu_3VS_4 (PDF 01-088-1318), $CuCrS_2$ (PDF 01-079-7417) and Cu_2MnS_2 (PDF 00-050-0540) are reported at the bottom of each of the panels, (see **Table S1** for more details).

In conjunction with XRD, HR-TEM along with the fast Fourier transform (FFT) evidence the single crystalline nature as well as the corresponding structures of all the three type of NCs, (**Figure 2,** top). HAADF-STEM with the corresponding EDXS elemental mapping highlight a uniform distribution of the elements in Cu_3VS_4 and $CuCrS_2$ NCs and a copper-rich surface for Cu_2MnS_2 NCs (**Figure 2,** bottom).

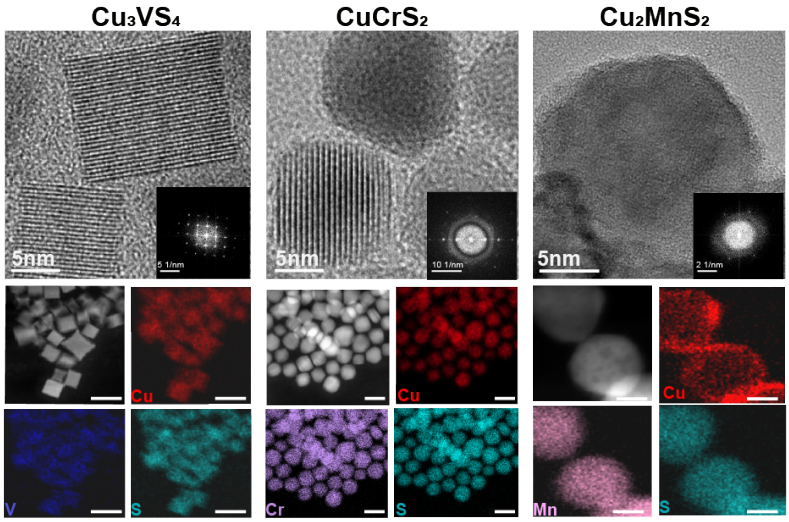

Figure 2. High-Resolution TEM images, along with the corresponding FFT, and HAADF-STEM images with EDXS elemental mapping of the Cu_3VS_4, $CuCrS_2$ and Cu_2MnS_2 reported in Figure 1. To note that a copper-rich surface is present in the case of Cu_2MnS_2. The scale bars in the HAADS-STEM images are 20nm for Cu_3VS_4 and $CuCrS_2$ and 10nm for Cu_2MnS_2.

Tuning the precursor reactivity

As we move from single to multicomponent NCs, a greater number of reaction paramenters needs to be thoroughly optmized because of the multiple and diverse interactions between different species. In particular, a reactivity balance among the metal precursors is essential to direct the synthesis towards the target compound while avoiding the competing formation of undesired byproducts, including single and binary species.[4,17,18] Based on computed oxophilicity and thiophilicity trends, Cu tends to form sulfur bonds more readily than V, Cr or Mn.[19] Thus, a stable copper precursor is desirable in order to retard/avoid the precipitation of Cu_xS (x=1,2) particles. On the other side, the oxophilicity (V>Cr>Mn) and thiophilicity (V<Cr<Mn) of the transition metal M should also be taken into account as binary M-O or M-S particles might form during the synthesis (**Figure S2**).[19]

We addressed the synthesis of Cu-M-S NCs by tuning the reactivity of the copper precursor while using DDT as the sulfur source, commonly employed to prepare chalcopyrite-type $CuInS_2$, $CuInSe_2$ and $Cu(In_{1-x}Ga_x)(S_ySe_{1-y})_2$ NCs,[20,21] and the same acetylacetonate precursors for the transition metal cations (i.e. $V(acac)_3$, $Cr(acac)_3$, $Mn(acac)_3$), the latter being common reagents, easy to handle and more organic soluble than other common salts.

The hard-soft acid-base(HSAB) theory is a good reference to anticipate the metal precursors reactivity.[4,17,18] At the same time, the metal-ligand bond energies should also be considered.[22] The copper precursors used in this work are: CuI, Cu(OAc) and $Cu(acac)_2$. As Cu^+ is a soft Lewis acid and I^- is a soft Lewis base, CuI is the most stable precursor among those considered in this work. OAc and acac are both hard Lewis bases. While acac is a harder base than OAc, Cu^{2+} is also a harder acid than Cu^+. Therefore, Cu(OAc) and $Cu(acac)_2$ are expected to exhibit similar reactivities based on the HSAB theory. Instead, DFT calculations evidence that the Cu-ligand bond energy is higher in $[Cu(OAc)]_2$ dimer and $[Cu(OAc)]_4$ tetramer complexes, which form in a non-coordinating solvent, such as ODE, than in $Cu(acac)_2$ (**Figure S3** and **Tables S2, S3**). All together, these considerations point at the following reactivity trend among the copper precusors $Cu(acac)_2$> Cu(OAc) >CuI.

Figure 1 and **Figure 3** illustrate that the copper precursor determines whether or not binary compounds form as intermediates during the synthesis.

In particular, in the case of Cu-V-S, CuI formed pure Cu_3VS_4 (**Figure 1A**); instead, Cu(OAc) and $Cu(acac)_2$ both led to the formation of Cu_xS, (x=1,2) and V_yO_z (y=2,5, z=3,9) species under the same reaction conditions, (**Figure 3A**, **S4**). Having an oxygen source in the synthesis, the formation of vanadium oxide is not surprising considering that V, being an early transition metal, has higher affinity for oxygen than for sulfur.

As for Cu-Cr-S, the pure $CuCrS_2$ phase formed with Cu(OAc) (**Figure 1B**); instead Cu_xS, (x=1,2) and Cr_kS_j, (k=2,3; j= 3,4) were detected by XRD with CuI and $Cu(acac)_2$ under same reaction conditions (**Figure 3B, S5**).

Similarly for Cu-Mn-S, $Cu(acac)_2$ led to the formation of phase pure Cu_2MnS_2 NCs (Figure 1C); instead impurities of Cu_xS, (x=1,2) and Mn_lS_m, (l=1, m=1,2) were found when CuI and Cu(OAc) were used as Cu precursors (**Figure 3C, S6**).

To note that both in the case of Cu-Cr-S and Cu-Mn-S, pure phase ternary compounds were eventually obtained but after much longer reaction times (**Figure S7)**.

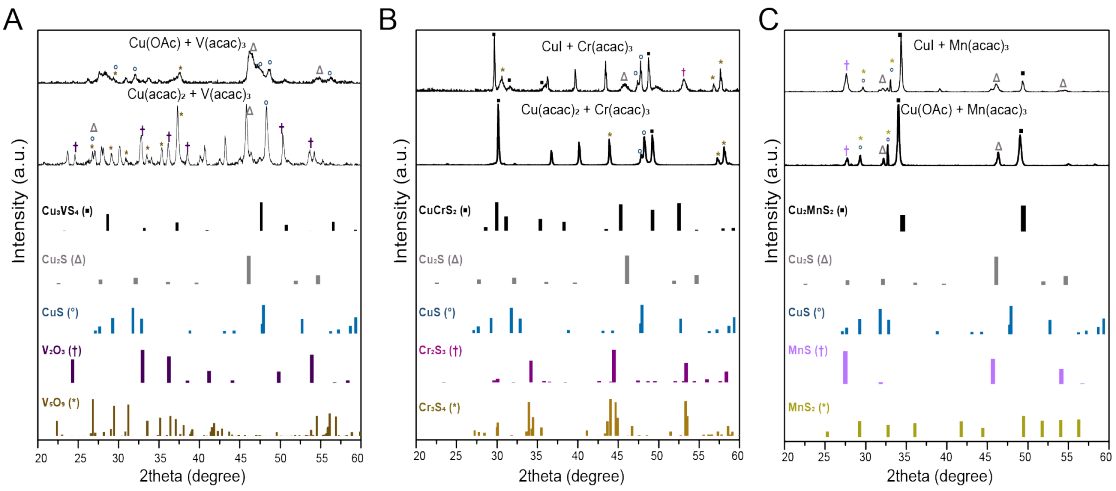

Figure 3. (A-C) XRD patterns of the samples obtained by reacting CuI, Cu(OAc) or $Cu(acac)_3$ with $V(acac)_3$, $Cr(acac)_3$ and $Mn(acac)_3$, respectively, at 280°C for 30minutes, while keeping unchanged all the other synthetic parameters. The reference patterns are reported at the bottom of the panel. ($CuCrS_2$, PDF= 01-079-7417; Cu_2MnS_2 PDF 00-050-0540; Cu_2S, PDF = 00-053-0522; CuS, PDF= 04-004-6505; Cr_2S_3, PDF= 00-011-0007; Cr_3S_4, PDF=01-089-0404; MnS, PDF = 00-040-1288; MnS_2, PDF= 00-025-0549).

Analysis of the reaction intermediates

At this point, it becomes interesting to investigate the mechanisms occurring during the formation of Cu_3VS_4, $CuCrS_2$ and Cu_2MnS_2 NCs in order to explain the different reaction rates depending on the Cu precursors. To this aim, we quenched the syntheses during the early stages and analyzed the as-obtained reaction intermediates by ex-situ TEM and XRD, (**Figure 4, S8-12)**.

Regarding Cu_3VS_4, the results relative to the reaction between CuI and $V(acac)_3$ (**Figure S8, S9**) overlapped with those of our previous work.[12] Here, Cu_xS (x=1,2) NCs and V-containing amorphous nanoparticles were found as the reaction intermediates eventually transforming completely into the final Cu_3VS_4 NCs after 30 minutes.

Interestingly, turning to $CuCrS_2$, we observed two different behaviors depending on the utilized Cu precursor (**Figure 4**, **S10)**. When CuI is reacted with $Cr(acac)_3$ (**Figure 4A**), the XRD data evidence the presence of binary copper sulfide from 3 minutes up to 4 hours. Additionally, immediately after the injection of the thiol source (DDT) a few peaks attributable to chromium sulfides are observed. If the more reactive Cu(OAc) is used instead (**Figure 4B**), the formation of the ternary phase is detected already after 1 minute from the injection, along with a sharp peak from the unreacted copper precursor, but no binary phases. Pure phase $CuCrS_2$ NCs are ultimately obtained after only 3minutes. A

similarly fast formation of the ternary NCs was observed for Cu_2MnS_2 in the reaction with $Cu(acac)_2$ as the Cu precursor (**Figure S11**).

Consistently with the XRD, the TEM analysis shows that the $CuCrS_2$ NCs are close to their final size already in the earlier stages of the synthesis, time helps only to better define the hexagonal shape (**Figure 4B, S10**). On the opposite, different morphologies coexist up to 4 hours for the synthesis with CuI (**Figure 4C, S5**).

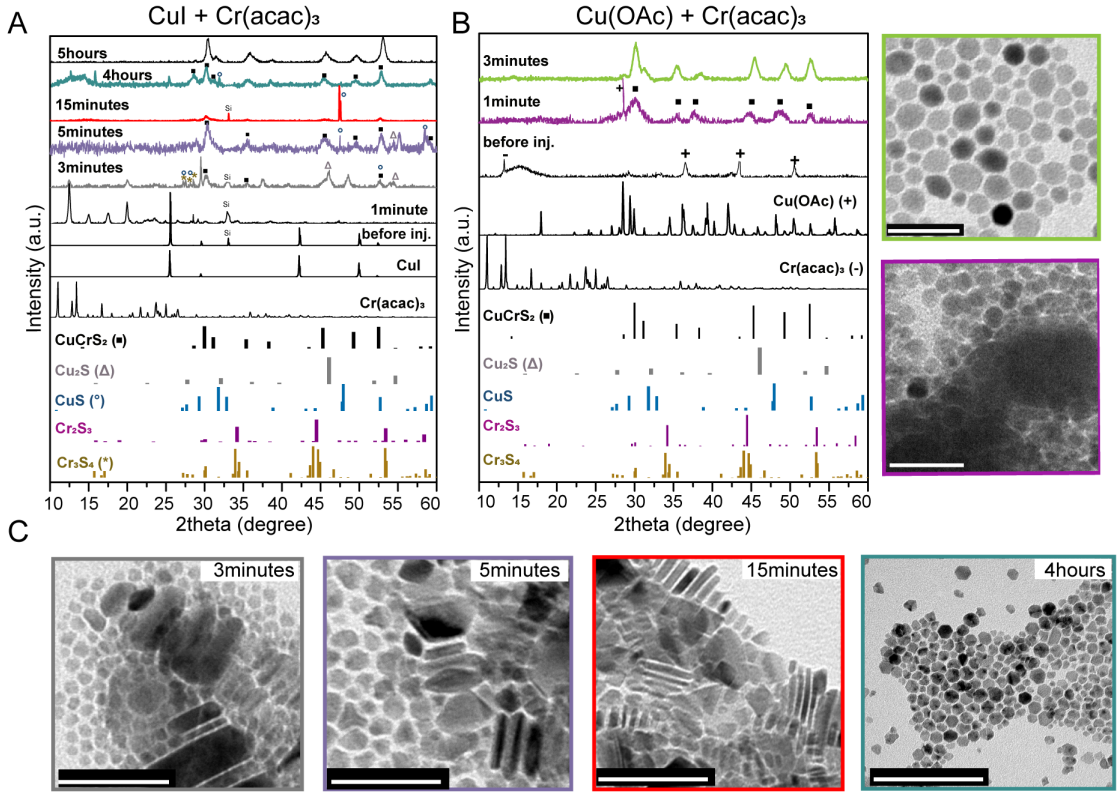

Figure 4. XRD patterns and TEM images of the aliquots extracted from the reaction flask at different times during the synthesis of $CuCrS_2$ performed using CuI, (A,C) and Cu(OAc) (B). The rest of the synthetic conditions were kept the same as described in the synthetic protocol. Reference patterns are reported at the bottom of each panel ($CuCrS_2$, PDF= 01-079-7417, Cu_2S, PDF = 00-053-0522; CuS, PDF= 04-004-6505; Cr_2S_3, PDF= 00-011-0007; Cr_3S_4, PDF=01-089-0404). In panel (A), the Si peak results from the substrate used during the measurements. A few peaks could not be assigned based on the crystallographic structures currently available in the database. The scale bars in the electron microscopy images are 25nm in panel (B) and 200nm in panel (C).

HAADF-STEM analysis and EDXS elemental mapping were performed on the reaction product collected after 3 minutes from the reaction between CuI and $Cr(acac)_3$ to get further insights into the composition of these reaction intermediates (**Figure 5, S12**).

These analyses suggest that the smaller size particles contain Cr and S. Interestingly, the bigger particles are composed of two distinct compositional domains, Cu_xS and Cr_yS_z, resembling hemispherical Janus particles, previously reported for other metal sulfide NCs.[23]

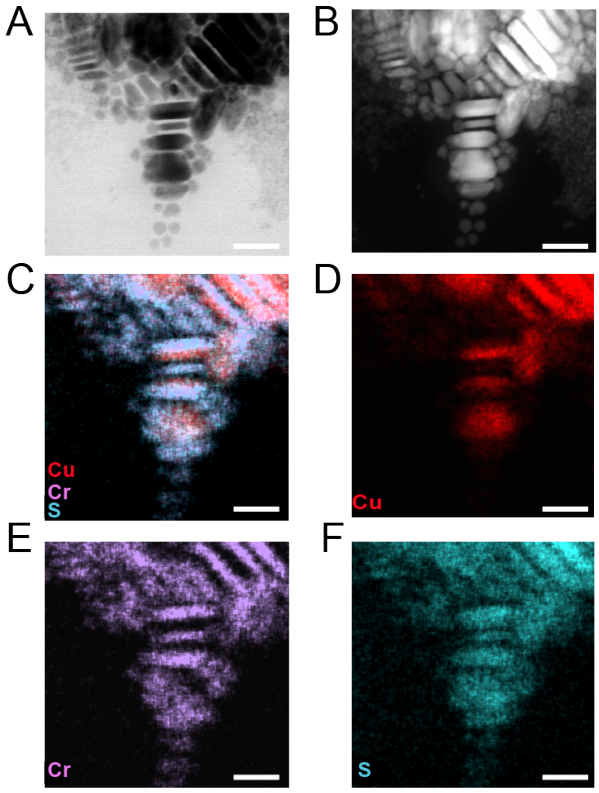

Figure 5. (A) Bright field TEM image, (B) HAADF-STEM image and (C-F) corresponding elemental mapping performed on the aliquot extracted after 3 minutes of reaction between CuI and $Cr(acac)_3$. The scale bars are 20nm.

Discussion on the reaction mechanism

The formation of multinary NCs can occur via direct nucleation from the precursor solution or via solid-state reaction among nanocrystalline precursors, the latter forming in-situ or pre-synthesized.[1,4,12,24,25]

Taking Cu-Cr-S as an illustrative case, when CuI or $Cu(acac)_2$ are used as the copper precursor, a solid state reaction between in-situ forming Cu_xS and Cr_yS_z NC intermediates

takes place. Because solid state diffusion must precede nucleation of the ternary compound, times longer than 90 minutes are needed to generate the $CuCrS_2$ NCs as a pure phase. Instead, when Cu(OAc) is reacted with $Cr(acac)_3$, $CuCrS_2$ NCs form as pure phase within one minute. While the occurrence of a very rapid solid-state reaction cannot be completely ruled out and future in-situ X-Ray spectroscopy experiments must be performed to obtain further insights, a direct route seems more likely.

Similarly for Cu-Cr-S, Cu_2MnS_2 is obtained via a solid state reaction with CuI and Cu(OAc), as in both cases Cu_xS and MnS_x (x=1,2) were detected as reaction intermediates, and via a direct route when $Cu(acac)_2$ is used. Cu-V-S is somehow unique because Cu_3VS_4 NCs form only via solid state reaction between amorphous V-containing nanoparticles and Cu_xS (x=1,2) when CuI is used as precursor.[12]

All together, these observations suggest that tuning the Cu precursor reactivity and properly balance it with the thiophilicity of transition metal is crucial to steer the reaction pathway. Particularly, balancing the intermediate thiophilicity of the Cr with the intermediate reactivity of the Cu(OAc) and the higher thiophilicity of the Mn with the higher reactivity of the $Cu(acac)_2$ favors the direct route. As for the Cu-V-S, because of the low thiophilicity of the V, only a Cu precursor even less reactive than CuI might form Cu_3VS_4 via a direct route. Nevertheless, in this case, the solid state reaction between the amorphous V-containing nanoparticles and the Cu_xS NCs occurs over relatively short timescale compared to the other systems. It is interesting to note that the formation of amorphous intermediates was found to facilitate the nucleation of phase pure ternary compound also in high temperature solid state reaction among elemental layers with atomic thickness.[26] A similar reasoning might explain our findings.

Interestingly, a narrower particle size distribution is measured in the case of the direct homogeneous pathway, rather than of the solid-state reaction (**Figure 6**). This result suggests that, in the former, the growth occurs in a focusing regime under diffusion control, while the solid state reaction might require the introduction of more uniform pre-synthesized NC precursors to improve the size distribution of the final NC product.

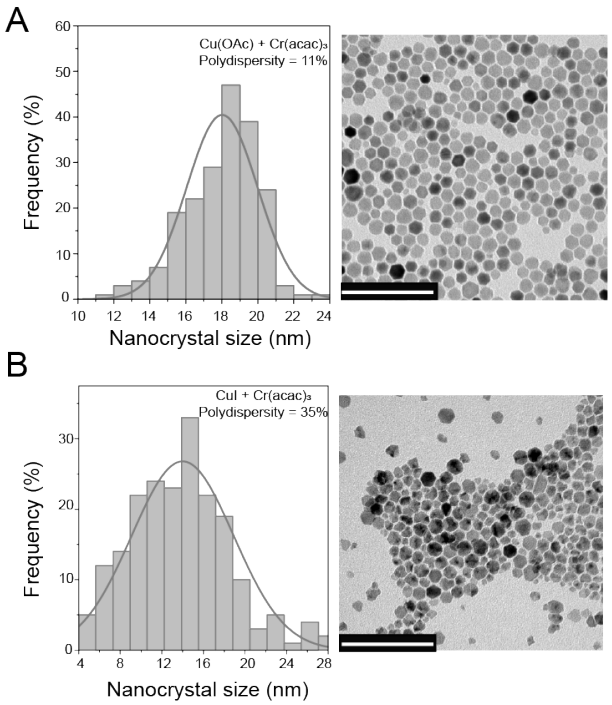

Figure 6. (A, B) Statistical size analysis and corresponding TEM images of the $CuCrS_2$ NCs obtained after reacting $Cr(acac)_3$ with Cu(OAc) for 30minutes and with CuI for 5 hours, respectively. The scale bars are 100nm.

CONCLUSIONS

In conclusion, we report for the first time on the synthesis and investigation of the reaction mechanisms behind the formation of colloidal Cu-M-S (M = V, Cr, Mn) NCs. We discovered that the choice of the copper precursor is key to obtain these ternary materials under the same reaction conditions, i.e. time/temperature/ligands/concentrations. In particular, a more reactive copper precursor must be used as the M cation thiophilicity increases. The resulting well balanced reactivity is translated into a faster solid-state reaction when less thermodynamically stable amorphous reaction intermediates form or into a direct homogeneous nucleation. Overall, our findings provide guidelines to obtain high quality ternary copper-based sulfides NCs, which is crucial to explore their physicochemical properties of interest for photovoltaics, thermoelectrics and theranostics.[15,27] In a more general context, this study represents a clear proof of the importance of the precursor chemistry to synthesize novel pure phase ternary compounds in low temperature "soft" synthesis approaches.

ASSOCIATED CONTENT

Supporting Information.

The Supporting Information is available free of charge via the internet at http://pubs.acs.org.

Experimental details, computational data, XRD and TEM results.

ACKNOWLEDGEMENT

This work was supported by the Swiss National Science Foundation (AP Energy Grant, project number PYAPP2_166897/1). JRP acknowledges the H2020 Marie Curie Individual Fellowship grant SURFCAT with agreement number 837378. The authors thank Dr. Anna Loiudice for helpful discussions.

REFERENCES

(1) Coughlan, C.; Ibáñez, M.; Dobrozhan, O.; Singh, A.; Cabot, A.; Ryan, K. M. Compound Copper Chalcogenide Nanocrystals. *Chem. Rev.* **2017**, *117*, 5865–6109.

(2) Gao, M. R.; Xu, Y. F.; Jiang, J.; Yu, S. H. Nanostructured Metal Chalcogenides: Synthesis, Modification, and Applications in Energy Conversion and Storage Devices. *Chem. Soc. Rev.* **2013**, *42*, 2986–3017.

(3) Leach, A. D. P.; Mast, L. G.; Hernández-Pagán, E. A.; Macdonald, J. E. Phase Dependent Visible to Near-Infrared Photoluminescence of CuInS2 Nanocrystals. *J. Mater. Chem. C* **2015**, *3*, 3258–3265.

(4) Yarema, O.; Yarema, M.; Wood, V. Tuning the Composition of Multicomponent Semiconductor Nanocrystals: The Case of I-III-VI Materials. *Chem. Mater.* **2018**, *30*, 1446–1461.

(5) Fan, F. J.; Wu, L.; Yu, S. H. Energetic I-III-VI2 and I2-II-IV-VI4 Nanocrystals: Synthesis, Photovoltaic and Thermoelectric Applications. *Energy Environ. Sci.* **2014**, *7*, 190–208.

(6) Haizheng Zhong,, Shun S. Lo, Tihana Mirkovic, Yunchao Li, Yuqin Ding, Yongfang Li, A.; Scholes, G. D. Noninjection Gram-Scale Synthesis of Monodisperse Pyramidal CuInS2 Nanocrystals and Their Size-Dependent Properties. *ACS Nano* **2010**, *4*, 5253–5262.

(7) Geisenhoff, J. Q.; Tamura, A. K.; Schimpf, A. M. Manipulation of Precursor Reactivity for the Facile Synthesis of Heterostructured and Hollow Metal Selenide Nanocrystals. *Chem. Mater.* **2020**, *32*, 2304–2312.

(8) Tappan, B. A.; Horton, M. K.; Brutchey, R. L. Ligand-Mediated Phase Control in Colloidal AgInSe2 Nanocrystals. *Chem. Mater.* **2020**, *32*, 2935–2945.

(9) Wu, X. J.; Huang, X.; Qi, X.; Li, H.; Li, B.; Zhang, H. Copper-Based Ternary and Quaternary Semiconductor Nanoplates: Templated Synthesis, Characterization, and Photoelectrochemical Properties. *Angew. Chemie - Int. Ed.* **2014**, *53*, 8929–8933.

(10) Luque, A.; Martí, A.; Stanley, C. Understanding Intermediate-Band Solar Cells. *Nat. Photonics* **2012**, *6*, 146–152.

(11) Vörös, M.; Galli, G.; Zimanyi, G. T. Colloidal Nanoparticles for Intermediate Band Solar Cells. *ACS Nano* **2015**, *9*, 6882–6890.

(12) Mantella, V.; Ninova, S.; Saris, S.; Loiudice, A.; Aschauer, U.; Buonsanti, R. Synthesis and Size-Dependent Optical Properties of Intermediate Band Gap Cu3VS4 Nanocrystals. *Chem. Mater.* **2019**, *31*, 532–540.

(13) Liu, Y.; Ding, T.; Luo, X.; Li, Y.; Long, J.; Wu, K. Tuning Intermediate-Band Cu3VS4 Nanocrystals from Plasmonic-like to Excitonic via Shell-Coating. *Chem. Mater.* **2020**, *32*, 224–233.

(14) Ghosh, S.; Avellini, T.; Petrelli, A.; Kriegel, I.; Gaspari, R.; Almeida, G.; Bertoni, G.; Cavalli, A.; Scotognella, F.; Pellegrino, T.; et al. Colloidal CuFeS2 Nanocrystals: Intermediate Fe d-Band Leads to High Photothermal Conversion Efficiency. *Chem. Mater.* **2016**, *28*, 4848–4858.

(15) Ke, K.; Yang, W.; Xie, X.; Liu, R.; Wang, L. L.; Lin, W. W.; Huang, G.; Lu, C. H.; Yang, H. H. Copper Manganese Sulfide Nanoplates: A New Two-Dimensional Theranostic Nanoplatform for MRI/MSOT Dual-Modal Imaging-Guided Photothermal Therapy in the Second near-Infrared Window. *Theranostics* **2017**, *7*, 4763–4776.

(16) Ramasamy, K.; Mazumdar, D.; Zhou, Z.; Wang, Y. H. A.; Gupta, A. Colloidal Synthesis of Magnetic CuCr2S4 Nanocrystals and Nanoclusters. *J. Am. Chem. Soc.* **2011**, *133*, 20716–20719.

(17) Buonsanti, R.; Milliron, D. J. Chemistry of Doped Colloidal Nanocrystals. *Chem. Mater.* **2013**, *25*, 1305–1317.

(18) Yarema, O.; Yarema, M.; Moser, A.; Enger, O.; Wood, V. Composition- And Size-Controlled I-V-VI Semiconductor Nanocrystals. *Chem. Mater.* **2020**, *32*, 2078–2085.

(19) Kepp, K. P. A Quantitative Scale of Oxophilicity and Thiophilicity. *Inorg. Chem.* **2016**, *55*, 9461–9470.

(20) Aldakov, D.; Lefrançois, A.; Reiss, P. Ternary and Quaternary Metal Chalcogenide Nanocrystals: Synthesis, Properties and Applications. *J. Mater. Chem. C* **2013**, *1*, 3756–3776.

(21) Reiss, P.; Carrière, M.; Lincheneau, C.; Vaure, L.; Tamang, S. Synthesis of Semiconductor Nanocrystals, Focusing on Nontoxic and Earth-Abundant Materials. *Chem. Rev.* **2016**, *116*, 10731–10819.

(22) Rhodes, J. M.; Jones, C. A.; Thal, L. B.; MacDonald, J. E. Phase-Controlled

Colloidal Syntheses of Iron Sulfide Nanocrystals via Sulfur Precursor Reactivity and Direct Pyrite Precipitation. *Chem. Mater.* **2017**, *29*, 8521–8530.

(23) Fenton, J. L.; Steimle, B. C.; Schaak, R. E. Tunable Intraparticle Frameworks for Creating Complex Heterostructured Nanoparticle Libraries. *Science (80-.).* **2018**, *360*, 513–517.

(24) Buck, M. R.; Bondi, J. F.; Schaak, R. E. A Total-Synthesis Framework for the Construction of High-Order Colloidal Hybrid Nanoparticles. *Nat. Chem.* **2012**, *4*, 37–44.

(25) Chen, P. C.; Liu, M.; Du, J. S.; Meckes, B.; Wang, S.; Lin, H.; Dravid, V. P.; Wolverton, C.; Mirkin, C. A. Interface and Heterostructure Design in Polyelemental Nanoparticles. *Science (80-.).* **2019**, *363*, 959–964.

(26) Anderson, M. D.; Thompson, J. O.; Johnson, D. C. Avoiding Binary Compounds as Reaction Intermediates in Solid State Reactions. *Chem. Mater.* **2013**, *25*, 3996–4002.

(27) Hansen, A. L.; Dankwort, T.; Groß, H.; Etter, M.; König, J.; Duppel, V.; Kienle, L.; Bensch, W. Structural Properties of the Thermoelectric Material CuCrS2 and of Deintercalated Cu: XCrS2 on Different Length Scales: X-Ray Diffraction, Pair Distribution Function and Transmission Electron Microscopy Studies. *J. Mater. Chem. C* **2017**, *5*, 9331–9338.